Investigation of the spatial distribution of sodium in bread microstructure using X-ray, light and electron microscopy

LWT - Food Science and Technology 209 (2024) 116787

Contents lists available at ScienceDirect

LWT

journal homepage: www.elsevier.com/locate/lwt

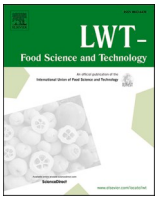

Investigation of the spatial distribution of sodium in bread microstructure using X-ray, light and electron microscopy

Simone Sala [a], Annika Altskär [b], Torben Nilsson Pingel [b], Alessandra Gianoncelli [c], Milan Žižić [c], Camille Rivard [d,e], Eva Olsson [f], Tim Nielsen [b], Niklas Lorén [b,*]

[a] RISE Research Institutes of Sweden, Dept. Manufacturing Processes, Lund, Sweden
[b] RISE Research Institutes of Sweden, Dept. Agriculture and Food, Gothenburg, Sweden
[c] Elettra Sincrotrone Trieste, SS 14 Km 163,5 in Area Science Park, 34149, Basovizza, Trieste, Italy
[d] Synchrotron SOLEIL, Gif-sur-Yvette, France
[e] INRAE, TRANSFORM, Nantes, France
[f] Department of Physics, Chalmers University of Technology, Gothenburg, Sweden

ARTICLE INFO

Keywords:
Sodium reduction
Food structure
Bread
X-ray fluorescence microscopy
Chemical analysis

ABSTRACT

The sodium consumption in many countries is too high, which results in increased risk for hypertension, cardiovascular diseases, stroke and premature death. Inhomogeneous sodium distribution using layering is a viable way to reduce sodium in bread that normally contains a lot of sodium. Prevention of sodium migration during production and storage is important for the function of this approach. Furthermore, the distribution of sodium between starch and gluten influences their properties. The spatial distribution of sodium was investigated at high resolution using combinations of X-ray fluorescence microscopy (XFM), scanning transmission X-ray microscopy (STXM), light microscopy (LM), scanning electron microscopy with energy-dispersive X-ray spectroscopy (SEM-EDX) and image analysis. Reference breads and layered bread samples were baked with one salt-free layer and one layer containing 3.6 wt% sodium chloride salt. The obtained results showed that the concentration of sodium is higher in the starch phase than in the gluten phase and that sodium migrates across the layer interface from the salt-containing to the salt-free layer. The ratios between the sodium concentration in the starch and gluten phases were dependent on the sodium concentration across the interfaces. Furthermore, magnesium and phosphor signals in bread yeast cells were observed using XFM.

1. Introduction

Excess salt (sodium chloride) consumption increases the risk of hypertension, thereby increasing the risk of cardiovascular diseases, stroke and other serious diseases (Grillo et al., 2019). Therefore, high sodium intake is a leading dietary risk factor for non-communicable diseases globally, measured both in terms of disability-adjusted life years and mortality rates over the past decades. In addition, excessive sodium consumption also leads to considerable economical costs for society ("Global Burden of Disease 2019," 2020), and prevention of early deaths by reducing sodium intake could save vast amounts of health care-related costs (Levy & Tedstone, 2017).

WHO and national authorities like the European Food Safety Authority (EFSA) NDA Panel (Turck et al., 2019) worldwide have issued recommendations for sodium consumption, specifically that sodium intakes for adults and children should be less than 2 g sodium per day (WHO, 2012). However, the consumption in most European Member States is close to twice this level. For this reason, WHO and the European Union have agreed a global target to reduce population sodium intake by 30% until 2025 for the prevention and control of non-communicable diseases (WHO, 2023). To meet demands from both authorities and consumers, and to be competitive, there is a strong need for the food industry to be able to offer reformulated products with lower sodium content.

However, sodium chloride is a crucial food ingredient with many important functions, and it is a challenge for the food industry to reduce sodium concentrations, without compromising sensory properties (e.g. taste, flavour and texture), microbial safety, shelf life and processability (Cepanec et al., 2017; Giese et al., 2019).

Many different strategies have been applied for reducing sodium

* Corresponding author.
E-mail address: niklas.loren@ri.se (N. Lorén).

https://doi.org/10.1016/j.lwt.2024.116787
Received 24 June 2024; Received in revised form 29 August 2024; Accepted 17 September 2024
Available online 17 September 2024

intake throughout the world. These have included reformulation of products, goals for maximum sodium content in specific product categories, reduction of sodium by stealth, information campaigns for increased awareness and education of the population, labeling legislation, and/or imposing taxes on products with a high sodium content.

When it comes to technical solutions for sodium reduction, several different approaches have been proposed. Unfortunately, there is not one universal solution for all types of food. One technical approach for sodium reduction that has been successfully applied is based on inhomogeneous distribution of the salt within the food matrix. This is a method that for instance is applicable on bread and other bakery products. Heterogenous salt distributions can be achieved by having layers with different salt content within the food, surface coating, using coated salt particles, or by creating spatially distributed compartments with different juiciness (Stieger, 2011).

The theory behind this approach is that human gustation is sensitive to fluctuations in salt concentration. This means that it is possible to obtain the same saltiness perception with a lower total sodium chloride content. It has been reported that the same perceived saltiness in white bread with 30% lower sodium content was obtained by baking in layers that differed in salt levels by a factor of ten (Noort et al., 2010). In a recent work, synergistic effects between acid addition and heterogeneous distribution of salt in bread has been demonstrated (Niimi et al., 2023). Reductions in the total salt concentration of the order of 40% were found. However, sodium reduction using concentration fluctuations requires that the sodium is inhomogeneously distributed after production and storage. (Niimi et al., 2023) investigated the sodium migration between the layers at the millimetre level using X-ray fluorescence microscopy (XFM). The results showed minor migration between the layers and establishment of a concentration gradient at the interface. However, not much is known about the detailed distribution of sodium in bread, if sodium distributes differently between starch and gluten, and if sodium is transported differently in the two phases.

Sodium chloride increases dough stability, saltiness and mixing time, decreases dough stickiness, and controls proofing (Beck et al., 2012). It influences gluten network formation and elasticity (Tuhumury et al., 2014) as well as starch gelatinisation (Nicol et al., 2019). During gelatinisation, starch starts to take up water causing the granules to swell and release amylose and amylopectin, which could influence the sodium distribution. To fully understand the function of sodium in bread baking, it is important to be able to analyse the spatial distribution of sodium with high spatial resolution. This is also key if strategies for heterogeneous distribution of sodium shall be used for salt reduction in foods.

Several analytical methods exist which are suitable to determine the content or distribution of sodium and other chemical elements within food samples. Methods based on mass spectrometry (MS) are routinely used in laboratories worldwide to determine the elemental content within analysed samples down to ppb in bulk. Spatially-resolved variations of MS exist such as laser ablation inductively coupled plasma mass spectrometry (LA-ICP-MS) which was recently applied to investigate the content of trace elements within wheat grains, achieving a spatial resolution down to tens of micrometres (Yan et al., 2020). Scanning electron microscopy with energy-dispersive X-ray spectroscopy (SEM-EDX) is routinely used to produce images with chemical contrast based on elemental composition and with spatial resolutions down to the nanometre range. However, the sensitivity of SEM-EDX is mostly suited to measure chemical elements present in wt% and its efficiency decreases for elements with low atomic number. X-ray fluorescence microscopy (XFM) is a chemical-contrast microscopy technique performing somewhere between MS and SEM-EDX: in fact, XFM uses a micro-focused X-ray beam to achieve spatial resolutions down to ~10 μm and is sensitive to elemental concentrations down to ppm. Even sub-micrometre focal spot sizes and sensitivity down to ppb can be achieved by performing XFM at high brilliance synchrotron radiation facilities (Castillo-Michel et al., 2017; Pushie et al., 2014). While absorption- and phase-contrast tomography at synchrotron sources has proven successful in the morphological characterisation of bread during proofing (Sun et al., 2020) and baking (Schott et al., 2023), application of other synchrotron-based materials characterisation techniques to food samples is still limited, and XFM in particular has been applied to raw materials, such as apples (Vidot et al., 2020), to analyse the spatial distribution of nutritious minerals in grains (Pongrac et al., 2013) and to detect metallic contaminants such as Cd in wheat grains (Yan et al., 2020) or Ti in lettuce (Larue et al., 2014) or cucumber (Servin et al., 2013). However, we have identified synchrotron-based XFM as a very suitable technique to accurately trace the distribution and concentration of sodium in the layered bread matrix down to sub-micrometre spatial resolution. In particular, this study relied on the soft X-ray microscopy beamlines TwinMic at Elettra Sincrotrone Trieste (Trieste, Italy) (Gianoncelli et al., 2016) and LUCIA at SOLEIL synchrotron (France) (Flank et al., 2006), as the micro-focused X-ray beams they offer are within the order of magnitude required to resolve the gluten network within the bread matrix (down to micrometre scale) and soft X-rays are most suited to trace chemical elements with low atomic number Z, such as sodium ($Z = 11$).The applicability of XFM is limited by the relatively short mean free path of soft X-ray photons such as those from Na fluorescence emission that dictates that all measurements must be carried out in a vacuum environment, which requires dry samples or advanced sample preparation. In addition, sample thickness is limited to a few micrometres to enable sufficient X-ray transmission for STXM measurements. Another limitation of synchrotron experiments in general is the limited access to synchrotron facilities and the long time between formulation of the research idea and execution of the synchrotron experiment.

The aims of this work are to determine the spatial sodium distribution in bread at micrometre level, investigate the distribution between starch and gluten phase of sodium, as well as analyse the sodium gradient at the interface between salt-containing layers and salt-free layers. In this work, first the microstructure of bread is presented. Subsequently, a method to determine the spatial sodium distribution in bread at micrometre level using XFM is shown and validated. Finally, results on the distribution of sodium between the gluten and starch phases as well as along the gradient are presented.

2. Materials and methods

2.1. Materials

For analysis at TwinMic (Gianoncelli et al., 2016), three bread types were baked, one layered bread and two references. The layered bread consisted of two layers: one coloured layer with 3.6 wt% salt, based on dry weight of flour, and one uncoloured layer without salt. The two reference breads were each baked from one of the doughs used in the layered bread. For analysis at LUCIA (Flank et al., 2006), bread samples were baked with three coloured layers with 3.6 wt% salt, based on dry weight of flour, alternated with three uncoloured layers without salt. For both bread batches, the food colouring was used to visually distinguish between the salt and salt-free layers. The total NaCl content in the layered breads at both TwinMic and LUCIA were 1.8 wt%, based on dry weight of flour.

The breads were baked with wheat flour containing 12.5% protein and 0.65% ash (Vetemjöl Starke Ex Bageri, Kobia, Sweden), commercial baker's dry yeast (Kronjäst Torrjäst för matbröd, Kronjäst, Sollentuna, Sweden), NaCl (Finkornigt hushållssalt 99.8% NaCl, Kryddhuset, Gothenburg, Sweden), red food colouring (Dr. Oetker Sverige AB, Gothenburg, Sweden, contains no NaCl) and pre-cooled water (6 °C). The baking forms were greased with a commercially available release agent for food products (Sprink, Bakels, Gothenburg, Sweden).

2.2. Baking

Two doughs, one coloured with salt and one uncoloured without salt, were prepared by mixing wheat flour, cold water, and dry yeast and kneaded slowly for 2 min in a dough mixer (NBT, Nordisk Bageriteknik, Sweden) and then further kneaded at a higher speed for 7 min and resting for 10 min. For the coloured dough with salt, NaCl salt was added between the two kneading steps. The two doughs were used for both the layered breads and the homogenous reference breads. Recipes for the two doughs are shown in Table 1.

For the LUCIA samples, the dough was initially rolled to about 2 cm thickness with a rolling pin, followed by rolling with a dough sheeter (Italos, Italy) to about 7–8 mm thickness. For the TwinMic samples, the dough was initially rolled to about 2.5 cm thickness with a rolling pin, followed by rolling with a dough sheeter (Italos, Italy) to about 20 mm thickness. For the layered breads the coloured dough was placed on top of the uncoloured dough.

In the layered breads for LUCIA, the thicker double layered doughs were cut into 9 pieces and for TwinMic into 6 pieces, each 12 × 6 cm long and wide. Three of these double layered pieces were stacked on top of each other resulting in three loaves, each with six layers of dough alternating in colour. The breads were carefully flattened with a rolling pin to about 4 cm thickness and further to between 3.3 and 3.5 cm thickness using the dough sheeter. The width of the dough was adjusted by cutting both sides with a metal spatula to obtain a width of 7 cm. The short sides on all doughs were cut to get a weight of around 330 g, the doughs were placed in baking tins which were greased with release agent. The doughs were proofed in a pre-conditioned proofing chamber (Sveba Dahlen, Fristad, Sweden) at 70% relative humidity (RH) and 37 °C for 60 min for further baking at 220 °C for 19 min (0% RH) in a convection oven (Sveba Dahlen, Fristad, Sweden).

In total, six breads of each type were baked for LUCIA and three breads of each type were baked for TwinMic. The baked breads were cooled for at least 90 min, cut in halves, packed in plastic bags, sealed and stored at −40 °C until further analysis.

2.3. Experimental design

For both synchrotron experiments, bread samples were analysed at different spatial positions to investigate the sodium gradient at the interface between the layers containing salt and the layers without salt, and the distribution of sodium between the starch and gluten phases. At TwinMic, four positions were selected, as shown in Fig. 1a and b, while at LUCIA five positions were selected, as shown in Fig. 1c. Table 2 summarises all samples analysed at TwinMic and LUCIA.

2.4. Sample preparation using cryo sectioning

For TwinMic, pieces 3 mm in width were cut for each sample (see Table 2). The bread pieces were quickly frozen on cryostat holders using Tissue Freezing medium cryoglue (Richmond, U.S.A). Ultralene film with thickness 4 μm (3525 Ultralene, SPEX SamplePrep, Metuchen, USA) was wrapped around microscopy glass slides and heated on a heating stage for glass slides (2208 Multiplate, LKB Bromma, Sweden). 3 μm thick sections were sectioned at −14 °C in a cryostat EM CM3050S (Leica, Vienna, Austria) and collected on the pre-warmed ultralene films.

For LUCIA, 5 μm thick sections from five areas (see Table 2) were sectioned at −14 °C in a cryostat CM 1900 (Leica, Vienna, Austria) and placed between two ultralene films with a thickness of 4 μm, on LUCIA's sample holders. The sections on ultralene film were mounted on holders specific for each beamline.

Table 1
Recipes for the doughs with and without salt.

	Dough with 3.6 wt% salt		Dough without salt	
Ingredient	w/w% on flour content	Weight	w/w% on flour content	Weight
Wheat flour	100	1292 g	100	1339.8 g
Water	50	660 g	50	660 g
Yeast	1.25	16.8 g	1.25	16.8 g
Food colour	–	2.4 g	–	–
Salt	3.6	47.5 g	–	–

2.5. Light microscopy

Light microscopy (LM) was used to select suitable areas in advance of analysis at each synchrotron facility. Images were also taken on sections after scanning with X-rays. At TwinMic, a digital optical LM (Keyence Serie VHX-7000 N microscope, Osaka, Japan) was used to check the mounted cryo sections and identify areas to scan with high-resolution XFM.

To verify the starch and the protein structures in the bread microstructure the cryo sections, 3 μm thick for TwinMic and 5 μm thick for LUCIA, were stained with Lughol's Iodine which stains the starch blue-purple and the protein yellow. The stained sections on ultralene film were analysed in a BX53F2 LM equipped with a CMOS colour camera SC50 (Olympus, Tokyo, Japan).

2.6. Confocal laser scanning microscopy

Pieces were cut from reference breads both with salt and without salt to visualise the microstructure in the bulk phase using a confocal laser scanning microscope (CLSM) (Leica TCS SP5 II, Wetzlar, Germany). The bread pieces were stained with Acriflavine for starch and Texas Red for protein. Acriflavine was excited at 488 nm and the emission recorded at 496–550 nm and Texas Red was excited at 594 nm and the emission recorded at 600–700 nm. Images were taken with a Leica HCX PL APO CS 63 × /1.20 water immersion objective with zoom 2, image size 1024 × 1024 pixels and scan rate 400 Hz.

2.7. SEM-EDX

Bread cryostat sections with a thickness of 5 μm were analysed by energy-dispersive X-ray spectroscopy (EDX) in a scanning electron microscope. To avoid charging issues, low-vacuum mode was used at 0.2 mbar water vapour pressure in a FEI Quanta 200 ESEM (Thermo Fisher Scientific Inc., USA). The slices were mounted with carbon tape on the sample holder and analysed with an acceleration voltage of 5 kV. Evaluation of the EDX data was conducted using the software AZtec (Oxford Instruments, UK).

2.8. X-ray fluorescence microscopy

Synchrotron-based XFM experiments on thin bread sections were carried out at two soft X-ray microscopy beamlines, namely LUCIA (Flank et al., 2006) and TwinMic (Gianoncelli et al., 2016). Both experiments were primarily aimed at locating Na from NaCl salt, while Cl could not be measured due to experimental constraints. Both beamlines feature silicon drift detectors (SDD) for measuring X-ray fluorescence emission within the vacuum experimental chamber. Motorised sample stages for controlled translation were used for XFM raster scans.

LUCIA was operated with an incident photon energy of 2250 eV suitable to detect O, Na, Mg, Al, and P. Such photon energy was selected to achieve optimal excitation of P and Na, but it should be noted that it was insufficient to excite Cl, whose absorption K edge is located at 2822 eV. Kirkpatrik-Baez (KB) mirrors were used to achieve a focal spot size of 2.6 × 2.4 μm^2 (H × V). A detector exposure time of 0.1 s per pixel and a scanning step of 2 μm were used throughout the measurements.

TwinMic was operated with an incident photon energy of 1515 eV

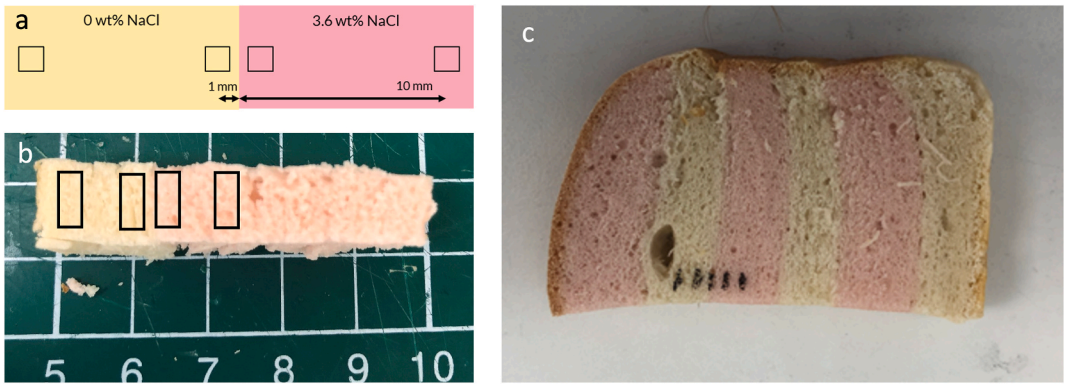

Fig. 1. Sampling positions in bread samples: sodium distribution was investigated around the interface between the salt containing layer and the salt-free layer. (a) Schematic illustration and (b) picture of TwinMic's bread. (c) Picture of LUCIA's bread. The black lines indicate there the sodium distribution was investigated.

Table 2
Nomenclature and description of samples for experiments at TwinMic and LUCIA.

Sample name	Description
TwinMic samples	
HighSalt1	About 1 mm from border in the salt layer
HighSalt10	About 10 mm from border in the salt layer
NoSalt1	About 1 mm from border in the salt-free layer
NoSalt10	About 10 mm from border in the salt-free layer
RefSalt	A homogenous bread with 3.6 wt% NaCl, evenly spread out in the whole bread
RefNoSalt	A homogenous bread with no added salt NaCl
LUCIA samples	
NoSaltCentre	In the centre of the salt-free layer, about 5 mm from the interface between the salt/salt-free layers
NoSaltEdge	In the salt-free layer, about 1 mm from the interface between the salt/salt-free layers
Interface	At the interface between the salt/salt-free layers
HighSaltEdge	In the salt-containing layer, about 1 mm from the interface between the salt/salt-free layers
HighSaltCentre	In the centre of the salt-containing layer, about 5 mm from the interface between the salt/salt-free layers

suitable to detect C, N, O, Na, and Mg. As for the experiment at LUCIA, the selected photon energy was insufficient to excite Cl which falls outside TwinMic's achievable energy range (400–2200 eV) and was therefore not detected. A focal spot size of 610 nm was obtained by using a gold Fresnel zone plate (FZP) with 600 μm diameter and 50 nm outermost zone width. A detector exposure time of 3 s per pixel was used throughout the measurements. A scanning step size of 500 nm was used to allow some illumination overlap between adjacent scanning positions. In addition to fluorescence signal, the transmitted X-rays were also recorded using a downstream CCD camera system and thus generating scanning transmission X-ray microscopy (STXM) images (Gianoncelli et al., 2006). This way maps of both attenuation and differential phase contrast were simultaneously obtained for the same pixels as the XFM elemental distribution maps. The simultaneous collection of STXM and XFM images enabled direct correlation between morphological and chemical maps.

For each experiment, multiple regions of interest (ROIs) were scanned for each position within the whole bread samples. ROIs were preselected based on LM images collected right before loading the samples at each beamline and adjusted based on coarse overview XFM or STXM scans performed with larger scanning step size and shorter detector exposure time: this approach strikes a balance between reducing radiation damage to each ROI before high spatial resolution scans and ensuring the suitability of the scanning positions. ROIs were selected so to cover flat areas – free from wrinkles and ripples – with abundant material – i.e. avoiding large pores and evident tears. At LUCIA, a total of 21 ROIs was scanned, covering an average area of 0.14 mm^2 per ROI and a total area of 3 mm^2. At TwinMic, a total of 13 ROIs was scanned, covering an average area of 1800 μm^2 per ROI and a total area of 24,000 μm^2.

For all XFM acquisitions, fitting of the X-ray fluorescence spectrum in each pixel of the maps was carried out using *PyMca*, a Python-based open source package developed for quantitative analysis of XFM datasets (Solé et al., 2007).

2.9. Image analysis

Image segmentation is a procedure aimed at separating different segments of a digital image and is typically used to isolate objects and identify boundaries. In this study, we applied image segmentation approaches to locate different phases – namely starch and gluten – within images from XFM, STXM and SEM-EDX. This was achieved by assigning a label to each pixel of each image. Three labels were used to represent starch, gluten and background, respectively. Every pixel not clearly associated to starch and gluten, is labelled as background, including for instance both dense particles contaminating the sample as well as empty regions due to the air pores occurring in baked bread. To minimise human bias, automated segmentation was carried out on all raw images first, followed by manual correction used to refine the initial labels. For the automated segmentation, thresholding proved sufficient. Thresholding consists of dividing the pixels of a digital image into two classes so that each pixel with an intensity above the chosen threshold is assigned one label and each pixel with an intensity below the chosen threshold is assigned another label. Within this study, Otsu's method was used to determine the intensity threshold for each image by maximising the variance between the two classes (Otsu, 1979). The implementation of this image segmentation approach is illustrated in Section 3.2.

3. Results and discussion

3.1. Microstructure of bread

The microstructure of bread obtained using different microscopy techniques is shown in Fig. 2. The microstructures of bread with 3.6 wt% salt (RefSalt) and without salt (RefNoSalt) are shown in the upper and lower rows, respectively. In the unstained images in Fig. 2a and d, starch is seen as transparent/white, and protein appears as darker areas; an example of a protein-rich area is annotated in green. In the sections for LM in Fig. 2b and e, gluten is stained yellow and starch granules are stained blue-purple. In the CLSM images of the gluten and starch phases in Fig. 2c and f, starch granules appear green, and the gluten network appears red. In general, large starch granules are elliptical and elongated, while small starch granules have a more spherical shape. During

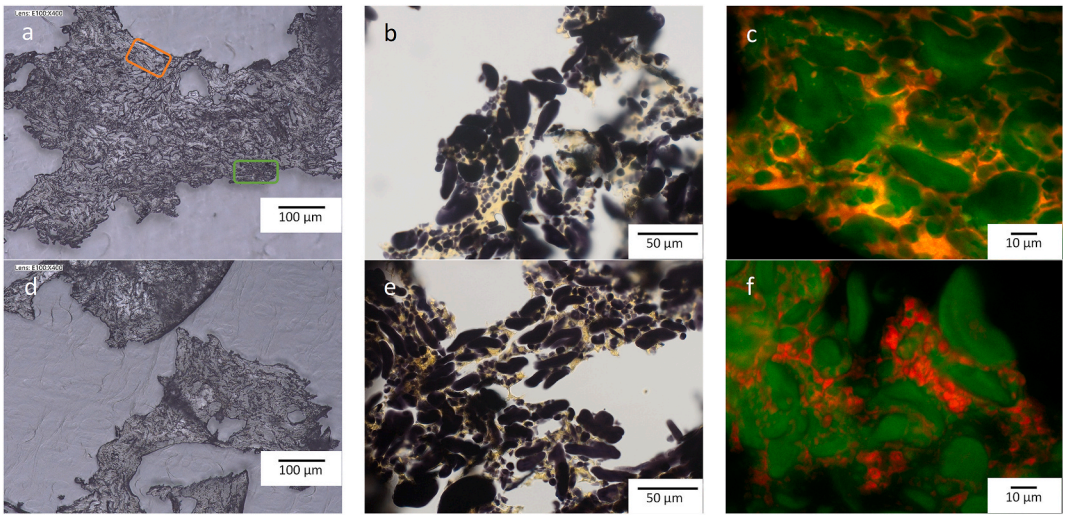

Fig. 2. Microstructure of bread: sample with 3.6 wt% salt (RefSalt) in the upper row and sample without salt (RefNoSalt) in the lower row. The micrographs are obtained with light microscopy and partially coaxial light 3D (a, d); light microscopy (b, e), and confocal laser scanning microscopy (c, f). In (a) and (d), starch is seen as transparent/white; example marked with an orange frame. Gluten appears as darker areas; example marked with a green frame. In (b) and (e), starch is stained blue-purple and protein is stained yellow. In (c) and (f), starch is green and protein is red. (For interpretation of the references to colour in this figure legend, the reader is referred to the Web version of this article.)

baking, starch takes up water, which deforms the shapes even further. The gluten network is surrounding the starch granules. When added salt is present, gluten is more homogenous and elongated. In the sample without salt, gluten is more heterogeneously distributed, and less connected.

3.2. Distribution of sodium between starch and gluten in bread

The applied strategy involved a combination of LM, XFM, STXM techniques and image analysis as well as validation using SEM-EDX. LM provides information about where starch and gluten are in the bread structure. STXM gives information about the local attenuation of the material. Since starch in general has a higher density than gluten and therefore attenuates X-rays more, STXM discriminates the location of starch and gluten in each sample. XFM provides spatially-resolved maps of the distribution of chemical elements of interest, such as sodium and nitrogen. As the nitrogen content is much higher in the gluten proteins than in the starch carbohydrates, nitrogen is used as a proxy to identify gluten in each sample. Therefore, a comparison of the XFM sodium and nitrogen maps with the STXM and LM images can reveal whether sodium is preferentially located in the gluten or in the starch phases in bread after baking. An example with 3.6 wt% salt (HighSalt10) is shown

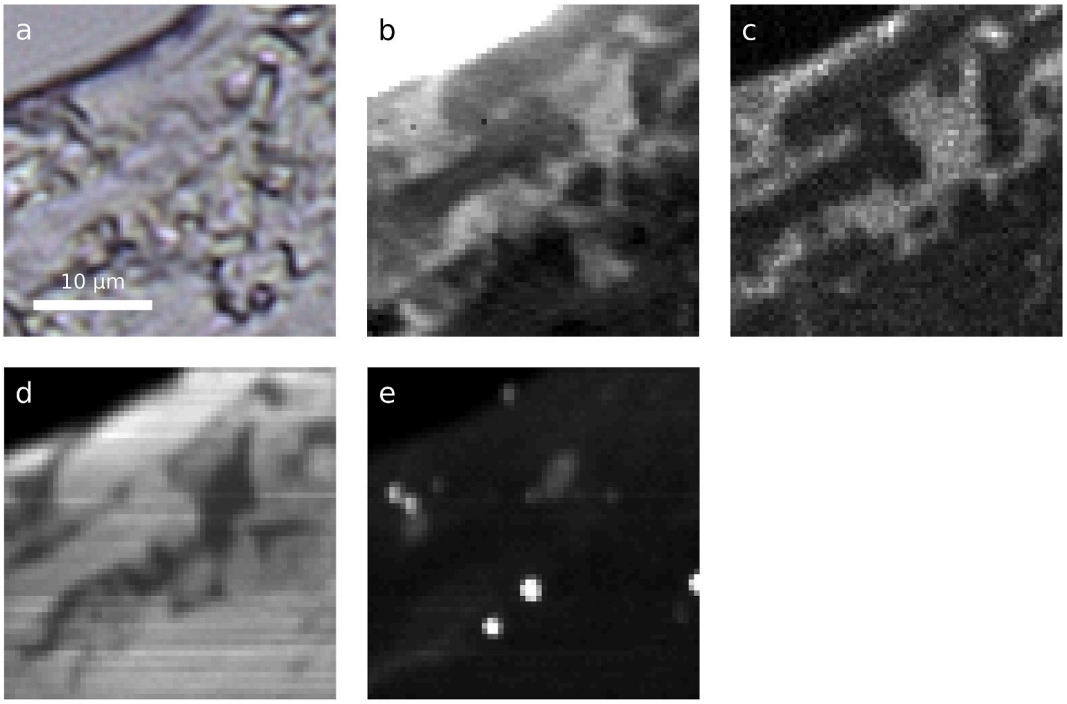

Fig. 3. Bread microstructure with 3.6 wt% salt (HighSalt10): (a) optical microscopy image (LM), (b) transmission image (STXM), (c) nitrogen distribution map (XFM), (d) sodium distribution map (XFM), (e) magnesium distribution map (XFM). The scalebar annotated in (a) is valid for all images as they originate from the same ROI. In the XFM maps (c, d, e), higher intensity (bright) corresponds to higher fluorescence signal for the respective chemical element.

in Fig. 3. Fig. 3a and b shows LM and STXM images, respectively, while Fig. 3c, d, and e show XFM distribution maps for nitrogen, sodium and magnesium, respectively. In the LM image (Fig. 3a) elongated starch granules can be distinguished from the surrounding gluten network. The same starch granules appear as darker regions in both the STXM image (Fig. 3b) and the XFM nitrogen image (Fig. 3c). The higher electron density of the starch granules leads to lower transmitted signal in the STXM image and their lower nitrogen content leads to lower fluorescence signal in the XFM nitrogen image. Therefore, a qualitative comparison between Fig. 3a–c and the XFM sodium image in Fig. 3d suggests that regions with a higher sodium fluorescence signal correspond to the location of the starch granules. In turn, this indicates that sodium is preferentially located in the starch phase. In addition, Fig. 3e reveals small (~1 μm) magnesium aggregates (bright spots), likely associated to yeast cells.

Quantitative analysis of each image requires labelling of its different portions via image segmentation. Fig. 4 shows an example of the automated segmentation carried out on the same area as in Fig. 3. First, Otsu's method was applied to the STXM image (Fig. 4a) to separate sample from background: result in Fig. 4b. Then, Otsu's method was applied to the nitrogen distribution map (Fig. 4c) from which the background was masked out, thus separating the gluten phase (rich in nitrogen) from the starch phase (poorer in nitrogen): result in Fig. 4d.

Fig. 5 illustrates the further manual refinement of these automatically generated labels. Based on visual inspection of both STXM (Fig. 5a) and XFM nitrogen (Fig. 5b) images, the automatically generated labels (Fig. 5c) were updated (Fig. 5d), for example labelling as background the uneven regions near pores to rule out edge artefacts. As a comparison, an overlay of the XFM nitrogen and sodium maps is shown in Fig. 5e.

After segmentation, the sodium content in the starch and gluten phases was extracted from each labelled image (Fig. 5d). Fig. 6a shows the original sodium map, while Fig. 6b and c displays the sodium in the starch and gluten phases after segmentation, respectively. Estimates of the sodium chloride (NaCl) salt concentration were obtained by normalising the projected sodium area mass density within different regions with respect to the known NaCl concentrations in the reference samples, i.e. 3.6 wt% and 0.0 wt% for the references with and without salt, respectively. The histogram from Fig. 6d illustrates the variation of NaCl salt concentration in the starch and gluten phases, revealing its higher abundance in the starch phase compared to the gluten phase.

The estimates of the spatially-resolved concentration of chemical elements detected by XFM are influenced by different factors. In these experiments, XFM images, were produced by raster scanning each sample on a plane perpendicular to the incident photon beam and thus obtaining 2D projections from a 3D sample. Formally, this generates projected area mass density maps which can be converted into elemental concentration maps assuming constant sample thickness within each scanned region. However, images obtained through such conversion are susceptible to artefacts in case of significant variations in sample thickness since the X-ray fluorescence emission signal from sodium is proportional to its amount in the probed volume. Fig. 7 displays two examples of cross sections of TwinMic samples obtained by LM that had a thickness of 3 μm. The thickness variation is minor and is independent of the phase, i.e. starch and gluten. Therefore, the observed variations of the sodium signal are likely not related to variations in specimen thickness. Other factors that influence the intensity of the fluorescence signal are the energy-dependent absorption cross section and atomic number Z-dependent fluorescence yield of each excited chemical element (Henke et al., 1993; Thompson, 2009). The emitted photons from nitrogen have lower energy, therefore they originate from a more superficial layer compared to the photons from sodium.

Finally, the segmentation procedure also bears an effect on the estimated sodium concentration within each phase. Boundary effects are particularly significant, as sodium concentration varies continuously across the boundary between each label (starch, gluten and background), due to diffusion but possibly also due to overlap in 3D between starch and gluten.

Measurements using SEM-EDX were carried out to independently analyse the sodium distribution in the bread structure. Fig. 8 shows the analysis performed on TwinMic's RefSalt sample with 3.6 wt% salt homogeneously distributed in the sample. Fig. 8a shows a SEM image of the bread structure. The starch granules are visible as slightly elongated and partly twisted structures. Fig. 8b and c shows the spatial distribution of sodium and nitrogen, respectively. Since gluten contains much more nitrogen than starch, Fig. 8c corresponds to the gluten distribution. A comparison between the sodium (Fig. 8b) and nitrogen (Fig. 8c) distributions clearly shows that more sodium is present in the starch phase. This is also supported by the SEM image in Fig. 8a where starch granules show a good correspondence with the sodium distribution from Fig. 8b.

Fig. 8d shows the segmentation generated from the nitrogen map (Fig. 8c): white corresponds to the gluten phase, black to starch. The intensities of the sodium signal in the black and white regions were calculated to determine how much more salt is present in the starch regions compared to the gluten regions. In this EDX map, the average sodium signal in the starch regions divided by the average sodium signal in the gluten regions corresponds to 1.57. This is in good agreement with a similar evaluation of the XFM data discussed in the following section (Fig. 11). Consequently, the measurements made by XFM and SEM-EDX validate each other and clearly show that sodium is preferentially located in the starch phase in TwinMic's RefSalt and HighSalt10 samples. The HighSalt10 samples are situated far from the boundary between the salt layer and salt-free layer and are expected to behave like the RefSalt samples.

3.3. Distribution of sodium across the salt/salt-free interface

In the previous section, the distribution of sodium between the starch and gluten phases in TwinMic's RefSalt and HighSalt10 samples has been shown. The results from both the combination of XFM, STXM and

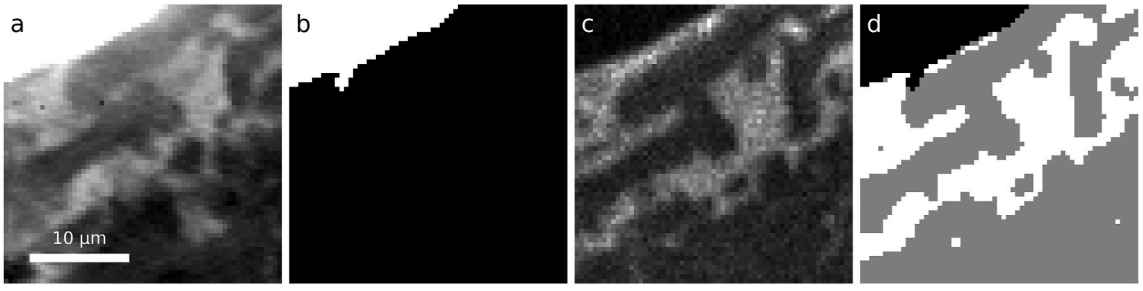

Fig. 4. Automated segmentation procedure (HighSalt10): (a) transmission image (STXM) used to segment out the background; (b) segmented background – white pixels are considered background and excluded from further segmentation; (c) nitrogen distribution (XFM) used to distinguish starch and gluten; (d) final segmentation – white pixels correspond to gluten and gray pixels correspond to starch. The scalebar annotated in (a) is valid for all images as they originate from the same ROI. In the STXM (a) and XFM map (c), higher intensity (bright) corresponds to higher transmission and fluorescence signal, respectively.

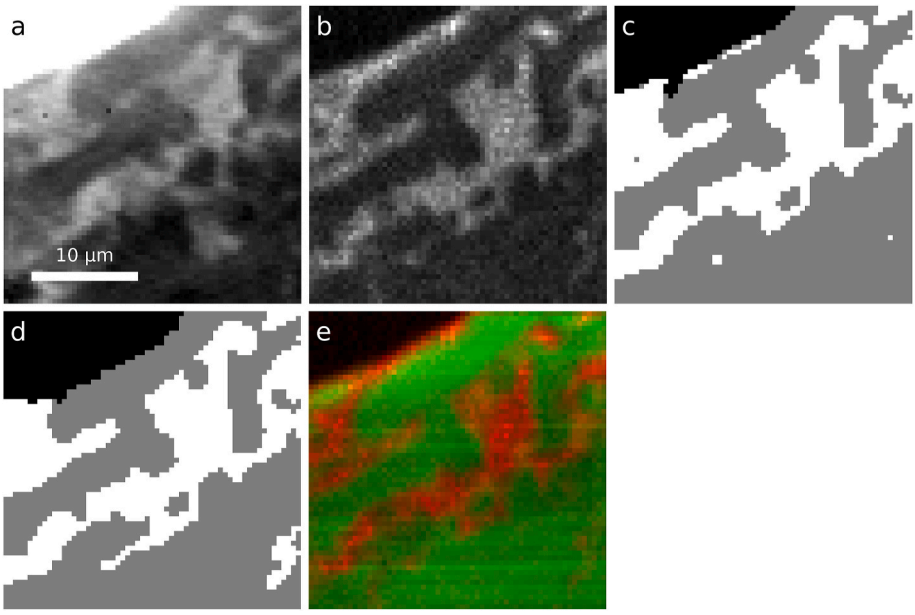

Fig. 5. Manual segmentation procedure (HighSalt10): (a) transmission and (b) nitrogen images as in Fig. 4; (c) labels resulting from automated segmentation and (d) final labels after manual refinement based on (a) and (b); (e) nitrogen (red) and sodium (green) overlay image. The scalebar annotated in (a) is valid for all images as they originate from the same ROI. (For interpretation of the references to colour in this figure legend, the reader is referred to the Web version of this article.)

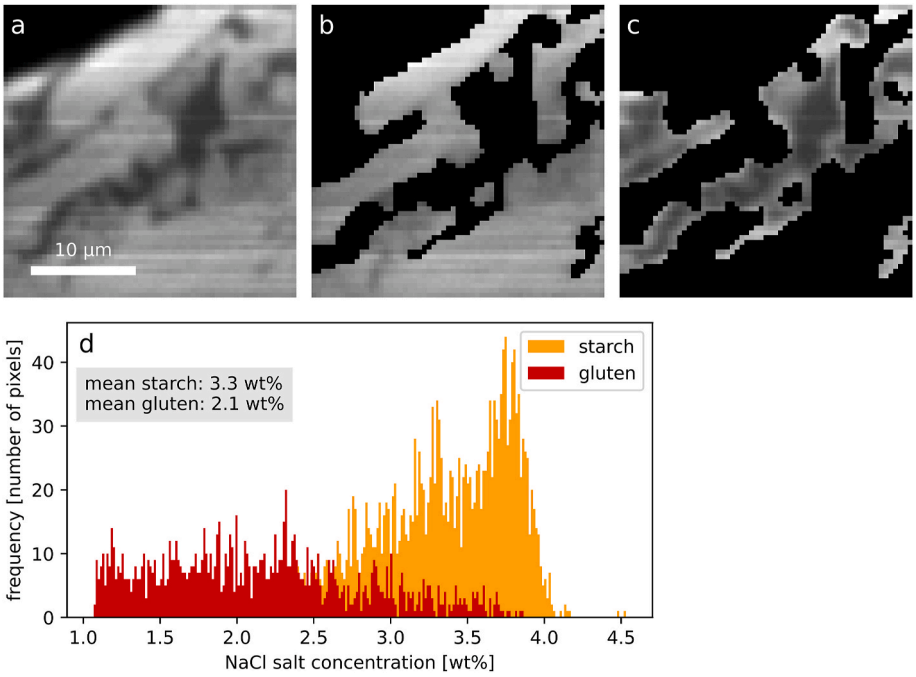

Fig. 6. Statistical analysis of sodium content in gluten and starch (HighSalt10): (a) original sodium map and (b) starch and (c) gluten portions resulting from segmentation, as in Fig. 5d; (d) histogram of sodium chloride (NaCl) salt concentration within starch (yellow bars) and gluten (red bars). The scalebar annotated in (a) is valid for all images as they originate from the same ROI. In the XFM maps (a, b, c), higher intensity (bright) corresponds to higher fluorescence signal for sodium. (For interpretation of the references to colour in this figure legend, the reader is referred to the Web version of this article.)

LM as well as SEM-EDX revealed that in these samples the sodium is preferentially located in the starch phase. Another interesting aspect is to investigate the sodium gradient across a salt/salt-free interface.

XFM scans were carried out at LUCIA on 21 ROIs (about 0.14 mm^2 each) sampling five different positions through the salt/salt-free interface (see Fig. 1c and Table 2), from well into the salt-free layer (NoSaltCentre) to well into the salt-containing layer (HighSaltCentre). Fig. 9 displays the concentration of sodium chloride (NaCl) salt extracted from XFM data of such regions revealing wide variations at the interface between the two layers.

The salt concentration specifically within gluten and starch phases was extracted from the segmented XFM images from TwinMic, sampling the positions represented in Fig. 1a and b. The estimated sodium concentrations across the salt/salt-free interface are shown in Fig. 10. Trends for the starch (Fig. 10a) and gluten (Fig. 10b) phases are similar, although for each position salt concentration in gluten is always lower than in starch. As expected, salt concentration is close to zero in the NoSalt10 sample and is high in the HighSalt10 sample, where it is in the

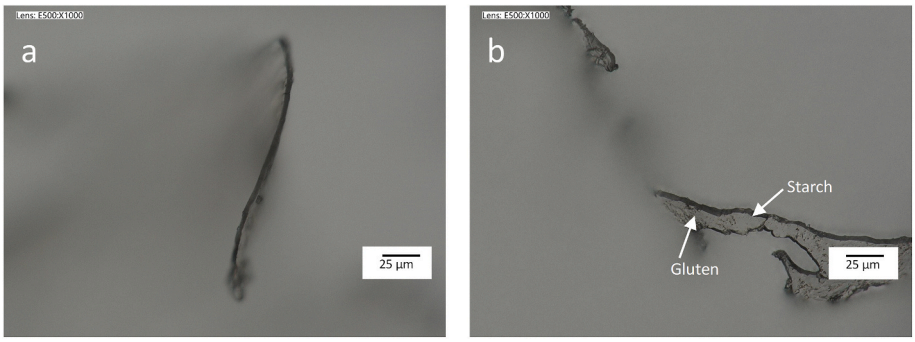

Fig. 7. LM images showing section thickness: (a) cross-section and (b) section with visible starch and gluten structures.

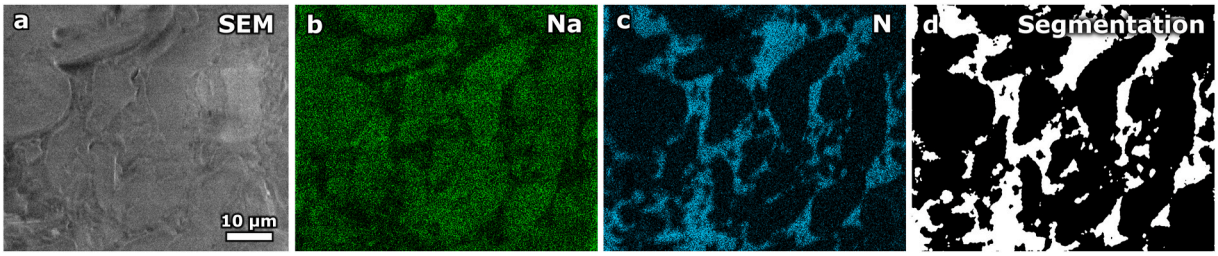

Fig. 8. Scanning electron microscopy (SEM) and energy-dispersive X-ray spectroscopy (EDX) images: (a) structure and distribution of (b) sodium and (c) nitrogen in the RefSalt sample with 3.6 wt% salt homogeneously distributed in the sample. (d) Segmented image based on the nitrogen map from (c): black corresponds to starch, white to gluten. The scalebar annotated in (a) is valid for all images as they originate from the same ROI.

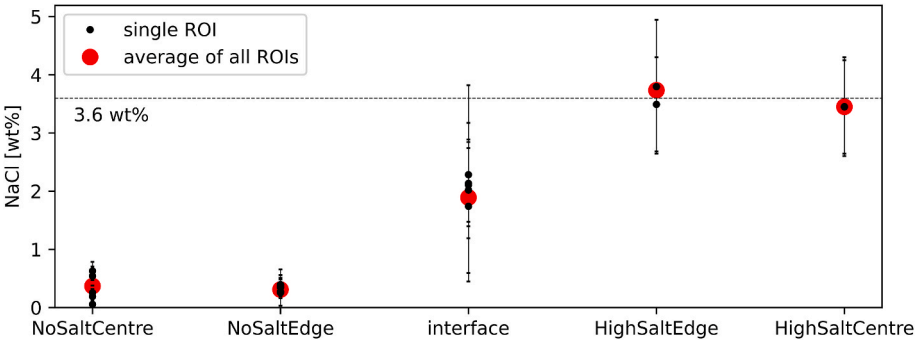

Fig. 9. Average concentration of sodium chloride (NaCl) salt across the salt/salt-free interface: obtained from whole regions of interest (ROIs) via XFM scans carried out at LUCIA; average concentration for each position is annotated as a red circle; error bars represent one standard deviation. (For interpretation of the references to colour in this figure legend, the reader is referred to the Web version of this article.)

range of 4–5 wt% in the starch phase. The HighSalt1 samples are also high in salt concentration and similar to the RefSalt and HighSalt10 samples. The NoSalt1 samples – taken in the salt-free layer, ~1 mm from the interface – have a salt concentration of about 2 wt% in the starch phase. This shows that sodium has migrated from the salt layer into the salt-free layer during processing and storage.

Note that the salt concentrations reported in Figs. 9 and 10 are calculated based on sodium content, as no direct information was accessible about chlorine. The ratios between the average concentrations of sodium in the starch and gluten phases are presented in Fig. 11. The ratios for RefNoSalt and NoSalt10 are close to one. However, sodium signal is very low in these samples, so the estimate of the ratios is rather uncertain. For the other samples with higher salt concentrations, the ratio between the average concentrations of salt in the starch and gluten phases is larger than one. This illustrates how sodium is preferentially located in the starch phase also across the salt/salt-free interface for the samples with larger amount of salt in accordance with the measurements shown in Fig. 6.

3.4. Location of yeast using XFM

Both XFM measurements at TwinMic and LUCIA were performed with an incident photon energy high enough to excite magnesium 1s electrons. At LUCIA, it was even possible to obtain distribution maps for phosphorus, as shown in Fig. 12. The structure in the magnesium maps mostly consists of circular regions a few micrometres wide (Fig. 12b and f). Yeast contains magnesium which is reported to be situated in the cell walls and the vacuole (Blackwell et al., 1995; Małgorzata et al., 2006). Phosphorus is abundant in yeast and is mainly associated with nucleic acids, phospholipids and proteins, but can also accumulate in polyphosphate which can be localized in the vacuole and other organelles, when phosphorus is abundant (Chen, 1999). The size and shape of the structures in the magnesium maps are most likely indicative of the spatial distribution of yeast. This hypothesis is further corroborated by the strong colocalization between the XFM phosphorus and magnesium distribution maps in Fig. 12b and c in the salt-free sample. In contrast, in the salt-containing sample, the XFM phosphorus and magnesium distribution maps in Fig. 12f and g are less colocalized, as apparent from

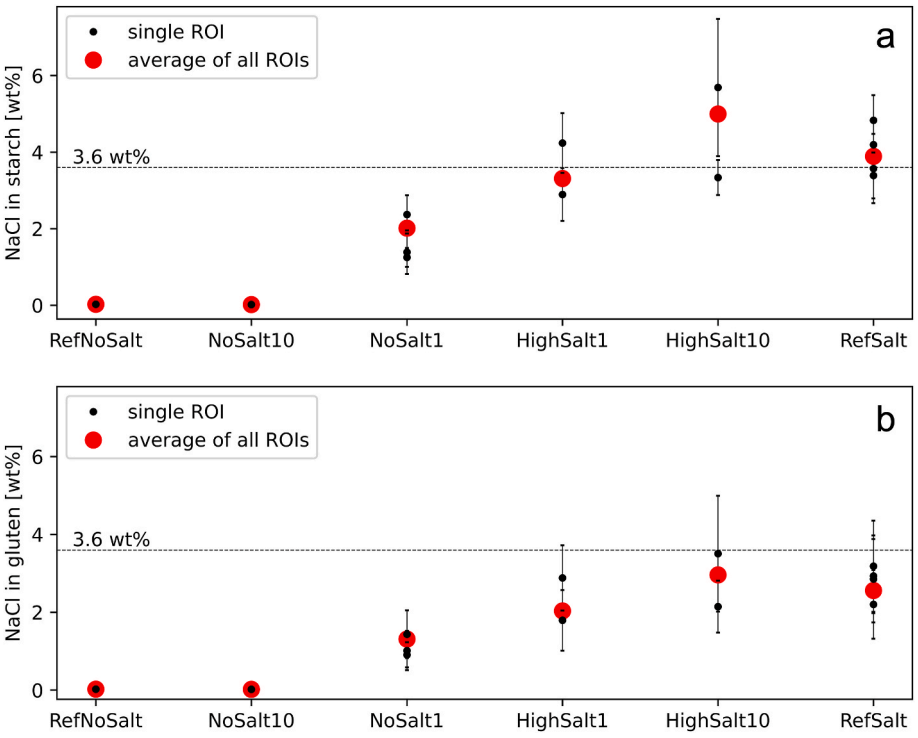

Fig. 10. Concentration of sodium chloride (NaCl) salt in (a) starch and (b) gluten phases: values obtained from XFM scans carried out at TwinMic on regions of interest (ROIs) on samples across the salt/salt-free interface, including references. Average concentration for each sample type is annotated as a red circle. Error bars represent one standard deviation. (For interpretation of the references to colour in this figure legend, the reader is referred to the Web version of this article.)

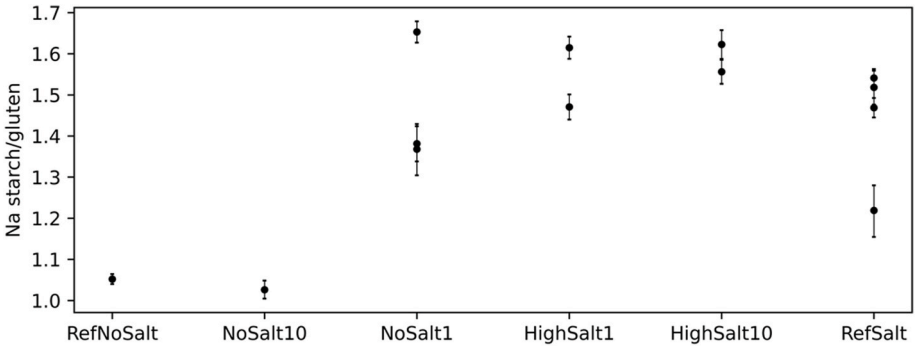

Fig. 11. Ratio between average concentration of sodium in starch and gluten phases: ratios for different samples obtained from Fig. 10. Error bars indicate a 95% confidence interval obtained via bootstrapping.

the overlay image in Fig. 12h. It is possible that magnesium has leaked out from the yeast cells under high salinity or due to cell lysis during the baking process. As a future work, it would be interesting to compare the magnesium distribution in the dough and the baked bread to investigate the effect of salinity on the time-dependent colocalization and diffusion of phosphorus and magnesium and to relate that to the baking properties.

4. Conclusions

The combination of X-ray fluorescence microscopy (XFM), scanning transmission X-ray microscopy (STXM), light microscopy (LM), image analysis and scanning electron microscopy with energy-dispersive X-ray spectroscopy (SEM-EDX) was found to be powerful to analyse the spatial distribution of sodium in bread. LM and the nitrogen signals from XFM and EDX provide information about the gluten protein structure. STXM, LM and SEM give information about the starch structure. By comparing images from LM and STXM, and XFM nitrogen maps with the XFM sodium maps, it was possible to determine the amount of sodium in the starch and gluten phases, respectively. These results were corroborated by comparing nitrogen and sodium maps from SEM-EDX data. It was also found that preparation of samples as thin sections with well-controlled thickness cryo-sectioning is crucial to obtain reliable results.

The results obtained via XFM, STXM, LM and SEM-EDX show that the concentration of sodium is higher in the starch phase than in the gluten phase. Sodium migrates across the salt/salt-free interface from the salt-containing layer to the salt-free layer. The ratios between the salt concentration in starch and gluten are in general larger than one across the salt/salt-free interface. It was also possible to identify the yeast cells in the bread using XFM. The application of these techniques to bread opens for both more detailed analysis of the effect of the spatial distribution of sodium and other ions on the final bread properties as well as mechanistic understanding of the role of ions in bread. It can also facilitate use of these techniques for other food science research questions involving ions such as understanding of mechanisms for gelation, chelation and complexation, development of methods to decrease iron deficiency, and

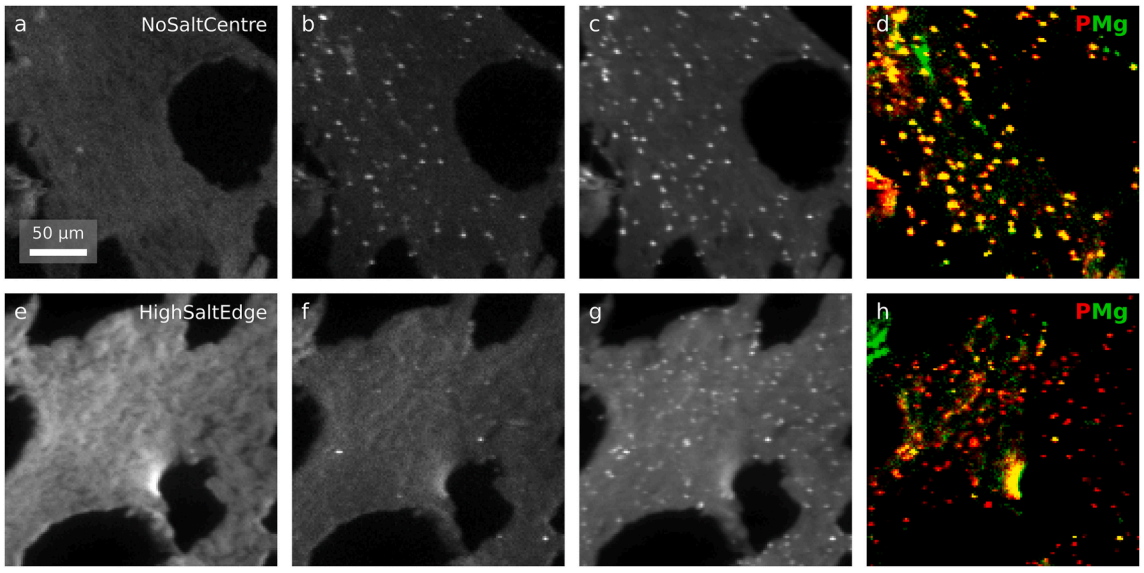

Fig. 12. Maps from XFM data measured at LUCIA on large regions: XFM maps from (a–d) NoSaltCentre sample and (e–h) HighSaltEdge sample. (a) and (e) represent sodium distribution: to enhance feature visibility, different colour scales have been applied to the samples with different sodium content. (b) and (f) represent magnesium distribution and (c) and (g) represent phosphorus distribution: the same colour scale has been applied for the same element. (d) and (h) phosphorus (red) and magnesium (green) overlay images: co-location of both elements results in yellow appearance. The scalebar annotated in (a) is valid for all images as they originate from ROIs of the same size. (For interpretation of the references to colour in this figure legend, the reader is referred to the Web version of this article.)

reduction of heavy metal content in foods.

CRediT authorship contribution statement

Simone Sala: Writing – review & editing, Writing – original draft, Visualization, Validation, Software, Methodology, Investigation, Formal analysis. **Annika Altskär:** Writing – review & editing, Writing – original draft, Visualization, Methodology, Investigation. **Torben Nilsson Pingel:** Writing – review & editing, Writing – original draft, Visualization, Software, Methodology, Investigation, Formal analysis. **Alessandra Gianoncelli:** Writing – review & editing, Software, Methodology, Investigation, Data curation. **Milan Žižić:** Writing – review & editing, Software, Methodology, Investigation, Formal analysis, Data curation. **Camille Rivard:** Writing – review & editing, Methodology, Investigation, Formal analysis, Data curation. **Eva Olsson:** Writing – review & editing, Resources, Conceptualization. **Tim Nielsen:** Writing – review & editing, Writing – original draft, Funding acquisition, Conceptualization. **Niklas Lorén:** Writing – review & editing, Writing – original draft, Project administration, Investigation, Funding acquisition, Conceptualization.

Declaration of competing interest

The authors declare that they have no known competing financial interests or personal relationships that could have appeared to influence the work reported in this paper.

Data availability

Data will be made available on request.

Acknowledgments

We acknowledge Elettra Sincrotrone Trieste for providing access to its synchrotron radiation facilities and for financial support under the IUS internal project. We acknowledge SOLEIL for provision of synchrotron radiation facilities. The fundings by the Swedish Research Council (VR) [2018–06378, 2018–06478], Sweden's innovation agency (Vinnova) [2020–01824] and FORMAS [2023–02010] are gratefully acknowledged.

References

Beck, M., Jekle, M., & Becker, T. (2012). Impact of sodium chloride on wheat flour dough for yeast-leavened products. I. Rheological attributes. *Journal of the Science of Food and Agriculture, 92*(3), 585–592. https://doi.org/10.1002/jsfa.4612

Blackwell, K. J., Singleton, I., & Tobin, J. M. (1995). Metal cation uptake by yeast: A review. *Applied Microbiology and Biotechnology, 43*(4), 579–584. https://doi.org/10.1007/BF00164757

Castillo-Michel, H. A., Larue, C., Pradas del Real, A. E., Cotte, M., & Sarret, G. (2017). Practical review on the use of synchrotron based micro- and nano- X-ray fluorescence mapping and X-ray absorption spectroscopy to investigate the interactions between plants and engineered nanomaterials. *Plant Physiology and Biochemistry, 110*, 13–32. https://doi.org/10.1016/j.plaphy.2016.07.018

Cepanec, K., Vugrinec, S., Cvetković, T., & Ranilović, J. (2017). Potassium chloride-based salt substitutes: A critical review with a focus on the patent literature. *Comprehensive Reviews in Food Science and Food Safety, 16*(5), 881–894. https://doi.org/10.1111/1541-4337.12291

Chen, K. Y. (1999). Study of polyphosphate metabolism in intact cells by 31-P nuclear magnetic resonance spectroscopy. In H. C. Schröder, & W. E. G. Müller (Eds.), *Inorganic polyphosphates: Biochemistry, biology, biotechnology* (pp. 253–273). Springer. https://doi.org/10.1007/978-3-642-58444-2_13.

Flank, A.-M., Cauchon, G., Lagarde, P., Bac, S., Janousch, M., Wetter, R., Dubuisson, J.-M., Idir, M., Langlois, F., Moreno, T., & Vantelon, D. (2006). LUCIA, a microfocus soft XAS beamline. *Nuclear Instruments and Methods in Physics Research Section B: Beam Interactions with Materials and Atoms, 246*(1), 269–274. https://doi.org/10.1016/j.nimb.2005.12.007

Gianoncelli, A., Kourousias, G., Merolle, L., Altissimo, M., & Bianco, A. (2016). Current status of the TwinMic beamline at Elettra: A soft X-ray transmission and emission microscopy station. *Journal of Synchrotron Radiation, 23*(6), 1526–1537. https://doi.org/10.1107/S1600577516014405

Gianoncelli, A., Morrison, G. R., Kaulich, B., Bacescu, D., & Kovac, J. (2006). Scanning transmission x-ray microscopy with a configurable detector. *Applied Physics Letters, 89*(25), Article 251117. https://doi.org/10.1063/1.2422908

Giese, E., Meyer, C., Ostermeyer, U., Lehmann, I., & Fritsche, J. (2019). Sodium reduction in selected fish products by means of salt substitutes. *European Food Research and Technology, 245*, 1651–1664. https://doi.org/10.1007/s00217-019-03277-1

Global Burden of Disease 2019. (2020). *The Lancet, 396*(10258), 1129–1306.

Grillo, A., Salvi, L., Coruzzi, P., Salvi, P., & Parati, G. (2019). Sodium intake and hypertension. *Nutrients, 11*(9), 1970. https://doi.org/10.3390/nu11091970

Henke, B. L., Gullikson, E. M., & Davis, J. C. (1993). X-ray interactions: Photoabsorption, scattering, transmission, and reflection at $E = 50$-30,000 eV, $Z = 1$-92. *Atomic Data and Nuclear Data Tables, 54*(2), 181–342. https://doi.org/10.1006/adnd.1993.1013

Larue, C., Castillo-Michel, H., Sobanska, S., Trcera, N., Sorieul, S., Cécillon, L., Ouerdane, L., Legros, S., & Sarret, G. (2014). Fate of pristine TiO2 nanoparticles and aged paint-containing TiO2 nanoparticles in lettuce crop after foliar exposure. *Journal of Hazardous Materials, 273*, 17–26. https://doi.org/10.1016/j.jhazmat.2014.03.014

Levy, L., & Tedstone, A. (2017). UK dietary policy for the prevention of cardiovascular disease. *Healthcare, 5*(1). https://doi.org/10.3390/healthcare5010009. Article 1.

Małgorzata, G., Stanisław, B., Joanna, R., & Wanda, D.-R. (2006). A study on Saccharomyces cerevisiae and Candida utilis cell wall capacity for binding magnesium. *European Food Research and Technology, 224*(1), 49–54. https://doi.org/10.1007/s00217-006-287-z

Nicol, T. W. J., Isobe, N., Clark, J. H., Matubayasi, N., & Shimizu, S. (2019). The mechanism of salt effects on starch gelatinization from a statistical thermodynamic perspective. *Food Hydrocolloids, 87*, 593–601. https://doi.org/10.1016/j.foodhyd.2018.08.042

Niimi, J., Ahlinder, A., Nilsson Pingel, T., Niimi, C., Höglund, E., Öhgren, C., Lorén, N., & Nielsen, T. (2023). Saltiness enhancement: Impact of acid added to bread with heterogeneously distributed sodium chloride. *Lebensmittel-Wissenschaft und -Technologie, 176*, Article 114557. https://doi.org/10.1016/j.lwt.2023.114557

Noort, M. W. J., Bult, J. H. F., Stieger, M., & Hamer, R. J. (2010). Saltiness enhancement in bread by inhomogeneous spatial distribution of sodium chloride. *Journal of Cereal Science, 52*(3), 378–386. https://doi.org/10.1016/J.JCS.2010.06.018

Otsu, N. (1979). A threshold selection method from gray-level histograms. *IEEE Transactions on Systems, Man, and Cybernetics, 9*(1), 62–66. https://doi.org/10.1109/TSMC.1979.4310076

Pongrac, P., Vogel-Mikuš, K., Jeromel, L., Vavpetič, P., Pelicon, P., Kaulich, B., Gianoncelli, A., Eichert, D., Regvar, M., & Kreft, I. (2013). Spatially resolved distributions of the mineral elements in the grain of tartary buckwheat (*Fagopyrum tataricum*). *Food Research International, 54*(1), 125–131. https://doi.org/10.1016/j.foodres.2013.06.020

Pushie, M. J., Cotelesage, J. J., & George, G. N. (2014). Molybdenum and tungsten oxygen transferases – structural and functional diversity within a common active site motif. *Metallomics, 6*(1), 15–24. https://doi.org/10.1039/c3mt00177f

Schott, F., Isaksson, S., Larsson, E., Marone, F., Öhgren, C., Röding, M., … Raaholt, B. W. (2023). Structural formation during bread baking in a combined microwave-convective oven determined by sub-second in-situ synchrotron X-ray microtomography. *Food Research International, 173*, 113283. https://doi.org/10.1016/j.foodres.2023.113283

Servin, A. D., Morales, M. I., Castillo-Michel, H., Hernandez-Viezcas, J. A., Munoz, B., Zhao, L., Nunez, J. E., Peralta-Videa, J. R., & Gardea-Torresdey, J. L. (2013). Synchrotron verification of TiO2 accumulation in cucumber fruit: A possible pathway of TiO2 nanoparticle transfer from soil into the food chain. *Environmental Science & Technology, 47*(20), 11592–11598. https://doi.org/10.1021/es403368j

Solé, V. A., Papillon, E., Cotte, M., Walter, P., & Susini, J. (2007). A multiplatform code for the analysis of energy-dispersive X-ray fluorescence spectra. *Spectrochimica Acta Part B: Atomic Spectroscopy, 62*(1), 63–68. https://doi.org/10.1016/j.sab.2006.12.002

Stieger, M. (2011). Texture-taste interactions: Enhancement of taste intensity by structural modifications of the food matrix. *Procedia Food Science, 1*, 521–527. https://doi.org/10.1016/j.profoo.2011.09.079

Sun, X., Scanlon, M. G., Guillermic, R.-M., Belev, G. S., Webb, M. A., Aritan, S., Nickerson, M. T., & Koksel, F. (2020). The effects of sodium reduction on the gas phase of bread doughs using synchrotron X-ray microtomography. *Food Research International, 130*, Article 108919. https://doi.org/10.1016/j.foodres.2019.108919

Thompson, A. (2009). *X-ray data booklet* (3rd ed.) https://xdb.lbl.gov/.

Tuhumury, H. C. D., Small, D. M., & Day, L. (2014). The effect of sodium chloride on gluten network formation and rheology. *Journal of Cereal Science, 60*(1), 229–237. https://doi.org/10.1016/j.jcs.2014.03.004

Turck, D., Castenmiller, J., de Henauw, S., Hirsch-Ernst, K., Kearney, J., Knutsen, H. K., , … Przyrembel, H., & EFSA Panel on Nutrition, Novel Foods and Food Allergens (NDA). (2019). Dietary reference values for sodium. *EFSA Journal, 17*(9). https://doi.org/10.2903/j.efsa.2019.5778

Vidot, K., Rivard, C., Van Vooren, G., Siret, R., & Lahaye, M. (2020). Metallic ions distribution in texture and phenolic content contrasted cider apples. *Postharvest Biology and Technology, 160*, Article 111046. https://doi.org/10.1016/j.postharvbio.2019.111046

WHO. (2012). Guideline: Sodium intake for adults and children. https://www.who.int/publications-detail-redirect/9789241504836.

WHO. (2023). WHO global report on sodium intake reduction. https://www.who.int/publications-detail-redirect/9789240069985.

Yan, B., Isaure, M.-P., Mounicou, S., Castillo-Michel, H., De Nolf, W., Nguyen, C., & Cornu, J.-Y. (2020). Cadmium distribution in mature durum wheat grains using dissection, laser ablation-ICP-MS and synchrotron techniques. *Environmental Pollution, 260*, Article 113987. https://doi.org/10.1016/j.envpol.2020.113987